Characterization of Fresh and Regenerated Industrial Hydrocracking Catalysts; Study Causes of Deactivation

Hajian Ghayemi, Salman; Samimi, Abdolreza*[+]

Chemical Engineering Department, Faculty of Engineering, University of Sistan and Baluchestan, PO Box 98164-161 Zahedan, I.R. IRAN

Nematollahi, Masoud

Process Engineer and Project Supervisor, Reserch and Development Department, Abadan Oil Refining Company, PO Box 6316953111 Abadan, I.R. IRAN

ABSTRACT: *In this investigation, fresh and regenerated Ni-W-Alumina-Zeolite industrial hydrocracking catalysts characterized via several analyzing methods, including XRF, XRD, BET adsorption, FT-IR, FESEM-EDS, and TGA-DTA to understand the phenomena affecting trend towards their deactivation. The XRD patterns represented the presence of main phases of Al_2O_3/Y-zeolite as support and $NiWO_4/WO_3$ as active compounds. For the catalysts subjected to a three-year reactor operation/regeneration cycle, the XRF analysis revealed elemental enhancement of Fe, Na, V, Pb, Sb, and S, mostly from outsources environment. The BET and BJH analyses represented cylindrical shape mesoporosity for the samples, while the total pore specific surface area and volume were reduced from 287.73 m^2/g and 0.46 cm^3/g to 160.84 m^2/g and 0.40 cm^3/g for fresh and regenerated samples, respectively. The latter results indicated possibly filling the pores with impurities and/or sintering of pores. By considering FESEM images, the smooth surface of the fresh sample and indented/corroded characteristics of the regenerated one were seen. The variety of analyses portrayed the increasing trend of the poisoning factors and the structural malfunction of the catalysts towards irreversible deactivation.*

KEYWORDS: *Ni-W catalyst; Deactivation; Poisoning; Sintering.*

INTRODUCTION

Hydrocracking is one of the main processes that convert the heavy oil materials to light ones, through the cracking of the molecules [1-3]. This is done by conducting a mixture of hydrogen and hydrocarbons towards a catalyst under controlled pressure and temperature. Concerning the chemical and physical properties, a wide variety of hydrocracking catalysts have been produced for refinery applications. The catalysts of hydrocracking can be monometallic such as Ni or Co, or bimetallic such as Ni or Co with other metals, i.e., Ni, Co, Mo, and W [4, 5]. The metals are well-dispersed on the supports including alumina, zeolite, or silica-alumina with a different content ratio [2, 3, 6, 7]. The choice of catalyst depends on the process that refinery is designed

* *To whom correspondence should be addressed.*
+ E-mail: a.samimi@eng.usb.ac.ir , samimi683@yahoo.co.uk
1021-9986/2021/6/1765-1776 12/$/6.02

for and properties of the feed of the refinery [8, 9]. Hydrocracking catalysts are bifunctional as hydrogenation and cracking functions, which work either all the while or consecutively on the feedstocks. Support is responsible for cracking reactions, which is carried out on its acidic sites. *Ferraz et al.* [10] were studied Ni-Mo sulfided catalysts, considering the same active phase content deposited on three types of supports, to analyze the role of the acidity of supports on the conversion of tetralin. They found that the acidity of support can promote the ring-opening of tetralin, and the yield of aromatics all over the reaction products using silica-alumina and alumina-Y zeolite support catalysts. On the other hand, hydrogenation function is done by the active metals phase. They are responsible for the completion of principle chemical reactions, aromatics hydrogenation, and preserving the catalysts not to be poisoned by the coke. *Pookte et al.* [11] were investigated a progression of fresh and deactivated Mo-Co industrial hydrocracking catalysts to study cyclohexene hydrogenation as a test reaction. They showed that hydrogenation activity of MO^{5+} in the catalyst could be identified depending on the sulfur content, using electron spin resonance characterizations.

Catalysts may be deactivated because of suffering from hydrocracking reactions. Deactivation of hydrocracking catalysts can occur in several ways, mainly coking, sintering, and contamination [12-17]. Coking is the main cause of deactivation of catalysts, which can become from the feedstock or occur during hydrocracking operation [14]. Coke deposits on the surface of the catalysts and results in pore volume loss [18, 19]. *Sahoo et al.* [20] employed a variety of characterization methods to investigate the formation of soft and hard coke in the spent catalysts. They demonstrated that the soft coke was generally made due to alkylated mono- and di-aromatics, and in less scale polyaromatics, while the hard coke was high in aliphatic substances. The second reason for deactivation of catalysts occurs by sintering and thermal degradation, which might be harmful to active phase structure and dispersal [14, 15, 21, 22]. The third one is the sedimentation of chemicals that are adsorbed on the active sites contaminating the catalysts [13, 14]. Contaminants such as V, As, Sb, Pb, Fe, and S are the main poisons that their adsorption reduces the activity and selectivity of the catalysts [15, 23]. V, As, Sb and Pb can come from the feedstock while Fe can be created by corrosion or erosion.

When a catalyst is deactivated, it needs to be regenerated under controlled conditions. Regeneration processes restore the activity and selectivity of catalysts. Since the cycles of hydrocracking operations are long-term periodic, therefore, the catalyst requires a careful regeneration operation. Regeneration operations may be achieved in two ways, including burning of the coke and redispersion of metals. The burning of the coke can be done by a flow of oxygen or air, which converts cock to CO_2 or H_2O based on the gas flow regeneration operation [21, 24]. There are several ways to regenerate the spent catalysts, such as oxidative regeneration, reductive regeneration, extractive regeneration, etc. The oxidative regeneration method is the most common and useful method used in industrial operations [25]. The oxidative method aims to restore the activity of deactivated catalysts by eliminating coke, utilizing oxidation. Dufresne and Brahma [26] expressed the essential wonders happening amid oxidative regeneration of hydroprocessing catalysts. Considering the lab test results, they found that the elimination of carbon and sulfur was a temperature-dependent process where the carbon was promptly removed in a single stage in the range of 300 and 450 °C. They also portrayed that the removal of sulfur was begun in the lower temperatures (i.e., 150 °C), and it ended just at temperatures above 600 °C. The burning of C and S was restricted by an oxygen diffusion impact into the pores of the catalyst. Teixeira da *Silva et al.* [27] used an industrial deactivated Ni-Mo/Al_2O_3 catalyst, which suffered many regeneration operations. The outcomes indicated that burning off the coke with an oxidizing blend, including little oxygen contents, was more productive in restoring the catalytic activity and textural characteristics of the used catalyst than reductive regeneration, continued by solvent extraction.

Due to the fact that the behavior study of the deactivation and regeneration of catalysts such as hydrocracking was investigated in different open literature. Therefore the main objectives of this paper are to distinguish comparatively the characteristics of the industrial catalysts obtained from an Iranian refinery and to describe the phenomena affecting the trend towards the deactivation of the regenerated catalyst. To understand how these characteristics influence the fresh and regenerated catalysts, several methods (i.e., X-Ray Fluorescence, X-Ray Diffraction, Brunauer-Emmett-

Teller adsorption, Fourier Transform InfraRed spectra, Field Emission Scanning Electron Microscopy-Energy Dispersive Spectroscopy, and Thermogravimetric analysis and Differential Thermal Analysis) have been employed.

EXPERIMENTAL SECTION

Catalysts Sample

The fresh and corresponding regenerated catalysts were obtained from the hydrocracking unit of an Iranian refinery. The fresh extruded catalysts were in the cylindrical shape of 1.4 mm diameter and 6 mm length and were made from nickel-tungsten oxide, supported on zeolite-alumina. The regenerated ones were selected from the partially deactivated catalysts which were subjected to a three-year reactor operation under the temperature of (380-440) °C, and the reactor inlet and outlet pressures of 2715 and 2640 psig, respectively. As recorded in the refinery logsheets, each stage of the regeneration process was carried out in the reactor under (400-440) °C using a mixture of oxygen-nitrogen gases for 7 days.

Characterization of Catalysts

The oxides form of fresh and regenerated hydrocracking catalysts was determined by XRF analysis using Spectro Xepos set up.

XRD patterns of fresh and regenerated catalysts were carried out in a Bruker Advanced D8 diffractometer, using Cu Kα radiation and operating at 55 kV, 60 mA and 1500 W, with $\lambda = 1.5408$ Å from 10° to 80° with a step time of 1 s and a step size of 0.010°.

To study the specific surface areas, pore diameters and pore volumes of the samples, N_2 adsorption/desorption isotherms were performed using a Microtrace BELSORP-mini II instrument. The two samples were degassed under 400 °C and vacuum of 10^{-5} Torr for 2 hours before the N_2 physisorption test. The Brunauer–Emmett–Teller (BET) method was used to compute the specific surface areas [28], and N_2 adsorption-desorption isotherms were applied to obtain the pore volumes of the samples. Desorption isotherms of N_2 physisorption were utilized to calculate the pore volumes of the fresh and regenerated catalysts by the Barret–Joyner–Halenda (BJH) method [29].

Chemical compositions were determined using a Fourier Transform InfraRed spectroscopy (FT-IR, Bruker Tensor II), which was equipped with the Platinum ATR Accessories with robust diamond crystal to determine the FT-IR bands of catalysts in the wavenumber range of (4000-400) cm^{-1} with 32 scans and 4 cm^{-1} resolution.

FESEM was employed to find the morphology of the samples using TESCAN MIRA 3-XMU with the energy of 15 kV, coupled with the EDS to obtain elemental spectra and mapping with 80000 magnification and 3 nm resolution.

The TGA-DTA was performed with the STA-504 thermal analyzer instrument. TGA-DTA of the fresh catalyst was performed in an O_2 gas atmosphere to obtain activity and resistance to the reactions when heated from ambient temperature to 1000 °C with a constant heating rate of 10 °C min^{-1} and a gas flow rate of 1 L hr^{-1}. On the other hand, the regenerated sample was subjected to TGA-DTA analysis in the Ar atmosphere from ambient temperature to 1000 °C with a constant heating rate of 10 °C min^{-1} and a gas flow rate of 1 L/h.

RESULTS AND DISCUSSION

Characterization techniques were used to obtain the properties of the catalysts. XRF was used to determine the elemental composition of catalysts. XRD was utilized to obtain the nature of crystalline phases. BET adsorption was carried out to calculate the specific surface area and pore volumes of the catalysts. Chemical compositions were determined using FT-IR spectroscopy. FESEM was aimed to study the morphology of the surface of the catalysts. Also, TGA-DTA was performed to characterize the thermal analysis.

XRF

In Table. 1, the oxide forms of fresh and regenerated catalysts are shown using the XRF method. As expected, Al_2O_3, SiO_2, NiO, and WO_3 are the main oxide forms of the samples as their elements make the main constituents of the catalyst's support and active agent composition. In the regenerated sample, Al_2O_3 remains almost unchanged, while SiO_2 decreases slightly. However, the WO_3 is reduced to about 9.56%, showing some extent of the catalyst deactivation. The elements of V, Sb, Pb, Fe, S, and Na oxides are expected to be the external source of the catalyst poisoning. As compared to the fresh catalyst, after several periods of catalyst reactor operation/regeneration, the Fe, Na, and S are still to some extent more in the regenerated ones. The increase of Na leads to raising the sintering of the catalysts, which is compatible with the

Table 1: Oxides form of the fresh and regenerated catalysts.

	Al_2O_3 %	SiO_2 %	NiO %	WO_3 %	Fe_2O_3 %	V_2O_5 %	PbO %	Na_2O %	SO_3 %	Sb_2O_5 %	LOI %
Fresh	15.14	13.69	11.57	43.34	0.03	0	0	0.99	0.16	0	13.72
Regenerated	15.16	12.93	10.36	39.19	0.046	0.001	0.001	1.551	5.847	0.01	14.56

results of *Lazić et al.* [30]. The existence of S may result in the formation of sulfide as a surface layer or bulk [31]. The V, Pb, and Sb do not exist in the fresh sample, but they are found in the regenerated one, which, as catalyst poisoning agents they can be transported from the feedstock into the catalyst. *Kohli et al.*, reported that the metals in the feed are deposited on the surface of catalysts, which these metals go into the pore cavity and block the active sites [32]. The latter result indicates that the trend of increase of these poisoning factors in the regenerated catalyst may lead to its complete deactivation.

XRD

XRD patterns of fresh and regenerated catalysts are shown in Fig. 1. Y-Zeolite, Al_2O_3, $NiWO_4$, and WO_3 are the main phases of both catalysts. As it is seen in the XRD patterns for both samples, Y-Zeolite and Al_2O_3 as key phases of the support are extensively the main crystalline matrix of the catalyst. Nevertheless, as compared to the fresh catalyst, the peaks of Al_2O_3 in the regenerated one are decreased, perhaps due to changing to the amorphous state. The XRD patterns reveal that for Al_2O_3 via the regeneration process, it is not possible to be returned to the prior state. Ni and W are the active metals of the catalyst which they are found in the form of NiO and WO_3 or $NiWO_4$ compounds. Although the NiO phase is essentially the main phase of nickel in the catalyst, it illustrates no peaks in XRD patterns of both fresh and regenerated catalysts, perhaps due to its amorphous nature, low content, or Ni bulky species [33]. *Adhikari et al.* also reported that the NiO did not exhibit peaks in the XRD patterns due to a lower amount [34]. On the other hand, WO_3, as the main phase of tungsten in the catalyst, depicts peaks extensively [35]. The $NiWO_4$ phase indicates peaks in both fresh and regenerated samples [36], but the peaks are diminished or shifted in the regenerated catalyst as compared to fresh one which it can be due to the loss of Ni and W. The presence of the excessive amount of tungsten oxide shows well distribution of tungsten on the support.

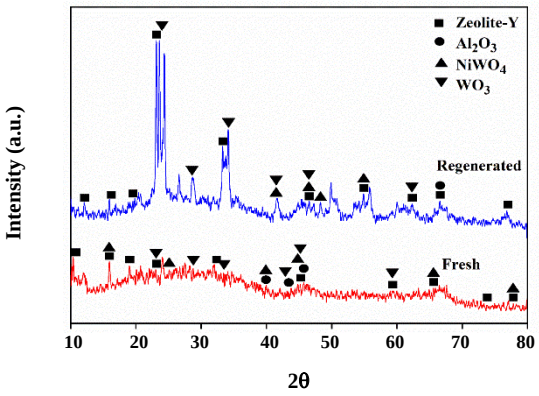

Fig. 1: XRD patterns of the fresh and regenerated catalysts.

N2 ***Adsorption/Desorption***

N_2 adsorption/desorption isotherms of fresh and regenerated catalysts are presented in Fig. 2, showing a type IV (IUPAC) isotherm and mesopore characteristics for both fresh and regenerated samples [37, 38]. No micropores exist in the fresh catalyst as no sharp slop is seen at low and middle pressures. The low and intermediate slope in the $P/P_0 \cong 0.005$-0.64 is an indication of the presence of mesopores structure in the catalyst [33]. An increase of slope above $P/P_0 = 0.64$, represents larger mesopores size [39]. There are no pores in the macroscale size range of the fresh catalysts because of no sign of Plato curve at $P/P_0 = 1$. Almost the same trend is seen for the regenerated catalysts, representing the domination of mesopores in their structure. However, the sudden increase in the slope is shifted to $P/P_0 = 0.75$ for the regenerated catalysts demonstrating a reduction in the volume of mesopores as compared to the fresh one. The hysteresis for both fresh and regenerated samples is H1, which again confirms the presence of mesopores [37, 38]. According to H1 hysteresis, the shape of the mesopores would be cylindrical with narrow pore size distributions. The results are in good agreement with those reported in the literature [39-41].

The pore volumes and BET surface areas of the fresh and regenerated catalysts are presented in Table 2. Furthermore, the cumulative and differential pore size distributions for both fresh and regenerated catalysts

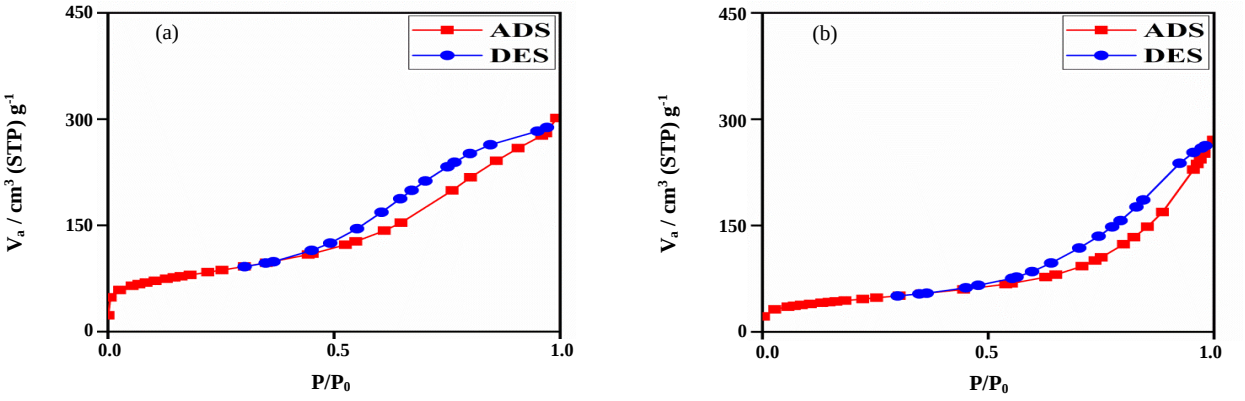

Fig. 2: N2 Adsorption/Desorption isotherms of (a) fresh and (b) regenerated catalysts.

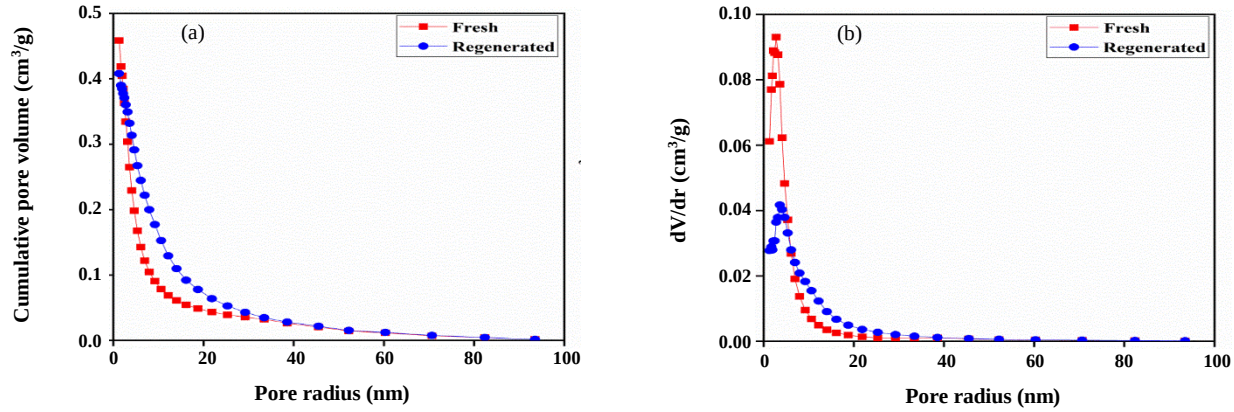

Fig. 3: BJH method (a) the cumulative pore size distribution and (b) The differential pore size distribution.

are illustrated, based on the BJH method, in Fig. 3. The pore size distributions of the catalysts affirm the existence of mesopores materials. As it is clear from Table 2, the specific surface area and total pore volume of the samples have been reduced from the fresh to regenerated catalysts, representing filling the pores with pollutant and waste materials and/or pores' sintering. Also, *Jahromi et al.*, reported that the reduction of the specific surface area of the regenerated catalyst was due to the formation of stable composition of Ni particles with the support of the catalyst during regeneration [42]. The Fig. 3 also shows the domination of mesopore size distribution in the catalysts, although the total pore volume has been reduced, relatively. A slight decrease in the pore volume of the regenerated catalyst compared to fresh one may be as result of the structural failure of support due to various factors such as corrosion.

FT-IR

The FT-IR studies were used to obtain specific information on molecular structure and chemical bonding. Fig. 4 explains the FT-IR spectra of fresh and regenerated catalysts. It indicates a broad band at 3366 cm^{-1}, which is associated with –OH stretch and the hydroxyl group. Furthermore, the bands at 1992 and 1640 cm^{-1} are attributed to the presence of OH bending vibration mode [43, 44]. The infrared regions of 1400-600 cm^{-1} correspond to tungsten-oxygen different modes [45]. This region confirms the existence of WO_3, which is one of the main active metal phases of the catalyst. The bands of 1333, 1200, 1143, 1074, and 602 cm^{-1} are illustrated the stretching vibration of W-O bonds [45]. The bands of 1333, 1200, 1143, and 605 cm^{-1} do not exist in the regenerated sample due to the reduction of tungsten in the fresh to the regenerated one. Furthermore, the bands of

Table 2: Properties of fresh and regenerated catalysts.

Sample	BET specific surface area (m^2 g^{-1})	Pore Volume (cm^3 g^{-1})
Fresh	287.73	0.46
Regenerated	160.84	0.40

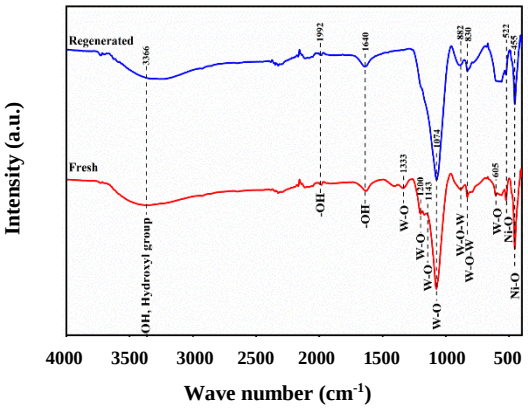

Fig. 4: FTIR spectra of the fresh and regenerated catalysts.

882 and 830 cm^{-1} belong to the stretching vibration of W-O-W bridge bonds [46, 47]. The bands at 502 and 455 cm^{-1} are assigned to Ni-O vibration for both fresh and regenerated samples [48, 49]. These pecks indicate the presence of NiO as another main active metal.

Morphology Study and Elemental mapping

Figs. 5 and 6 present the FESEM images of fresh and regenerated hydrocracking catalysts, respectively. By comparing the images, it can be seen that the surface of the fresh sample is smooth, in contrast for the regenerated one, the surface has been indented and corroded after the reactor operation mainly due to the collisions of the catalysts with each other and reactor walls. In the regenerated sample, some more white particles are observed, which would be a result of the presence of toxic particles. The latter observation would illustrate an increasing trend of the catalysts toward the irreversible deactivation after a large number of reactor operations.

The elemental characterization was carried out on fresh and regenerated catalysts using the EDS analyze, as shown in Fig. 7, respectively. EDS analyses portrayed the lower amount of Ni and W in the regenerated sample than the fresh one. The lessening of W would be due to the reaction of tungsten with sodium, which led to the production of sodium tungsten oxide. Fe and S are still in more amounts in the regenerated sample compared to the fresh sample after regeneration, due to the reduced nature of the elements, by combining with oxygen. Sulfur may result in the formation of Ni_3S_2, which can restructure the surface of the catalyst and a variety of electron density in the active metal [31]. The oxide amount of these elements over time and after several regeneration operations, are further increased, leading to completely deactivation of the catalyst.

The elemental mapping was also applied to find out the distribution of elements of support and active metals phase for both fresh and regenerated catalysts. Fig. 8 illustrates the distribution of the support elements, Al, O, and Si, in the fresh and regenerated catalysts. As it is clear, these elements are well-dispersed in both fresh and regenerated samples. However, the amounts of Al and O have been decreased in the regenerated catalyst because of partial demolition of the support by the deactivation factors. Fig. 9 represents the elemental mapping of Ni and W, indicating their reduction in the regenerated sample as compared to the fresh one. This reduction would be due to corrosion and erosion of the catalyst in the reactor or their combination with other deactivation elements. Also, the FESEM-EDS elemental mapping shows that Ni and W were well distributed in the catalysts. The elemental distribution of Fe and S is seen in Fig. 10 for both fresh and regenerated catalysts. The amount of S is considerably increased in the regenerated catalyst due to the deposition from the feedstock, and Fe is slightly raised as a result of deposition on the catalysts surface from outsources Fe. Both Fe and S are the main deactivation poisons for the catalysts, and their higher amounts after a three-year cyclic regeneration is an indication of the irreversible deactivation trend of the catalysts.

Thermal analysis

The TGA-DTA was used to determine the activity and resistance of fresh sample under the O_2 atmosphere to the reaction, as well as its thermal stability. The TGA-DTA results of the fresh sample are shown in Fig. 11, in which three

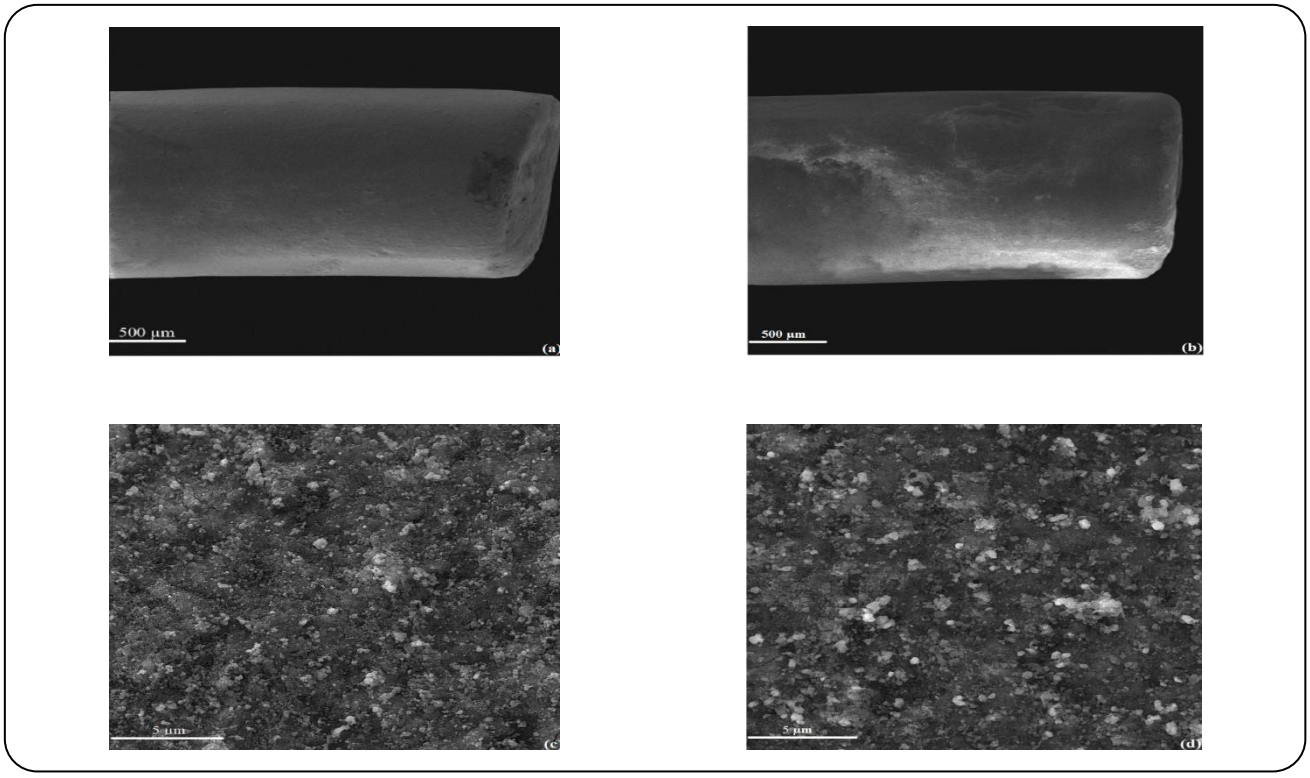

Fig. 5: FESEM images of the catalysts; (a) Fresh-500 µm, (b) Regenerated-500 µm, (c) Fresh-5 µm and (d) Regenerated-5 µm magnifications.

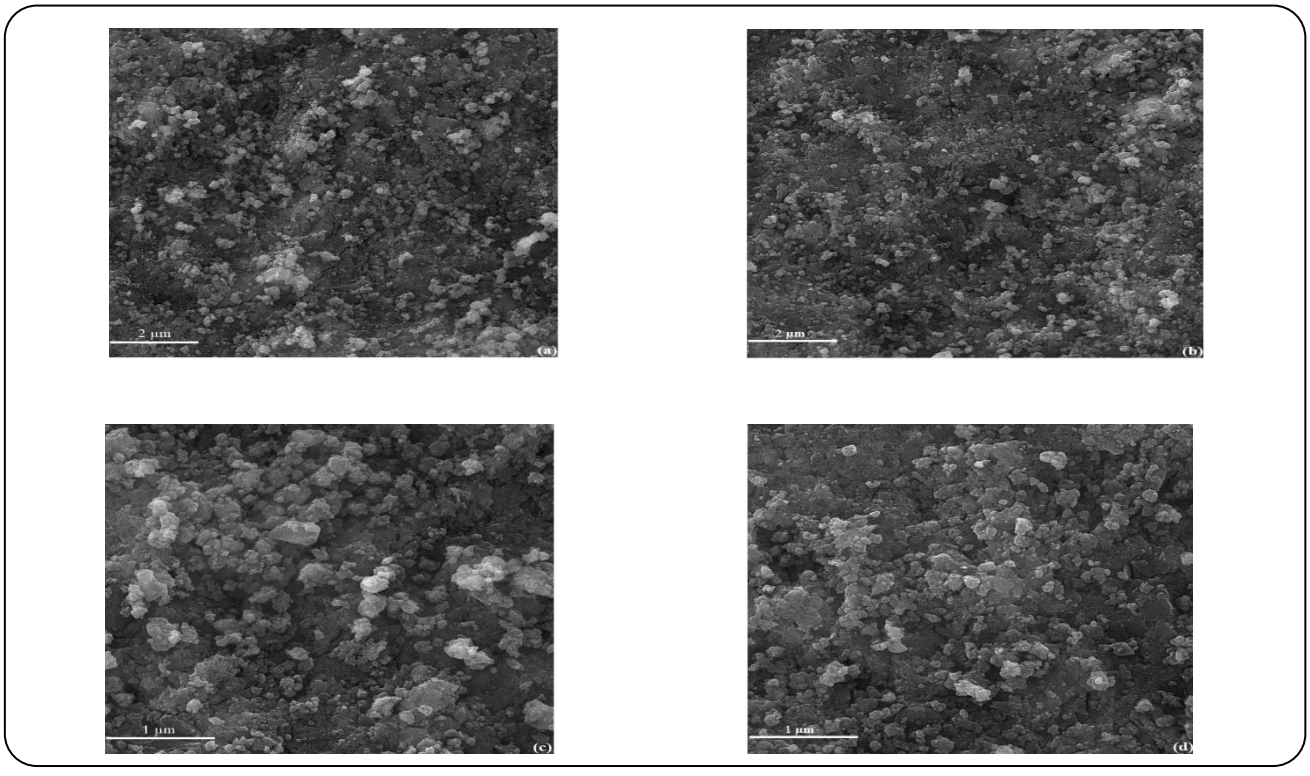

Fig. 6: FESEM images of the catalysts; (a) Fresh-2 µm, (b) Regenerated-2 µm, (c) Fresh-1 µm and (d) Regenerated-1 µm magnifications.

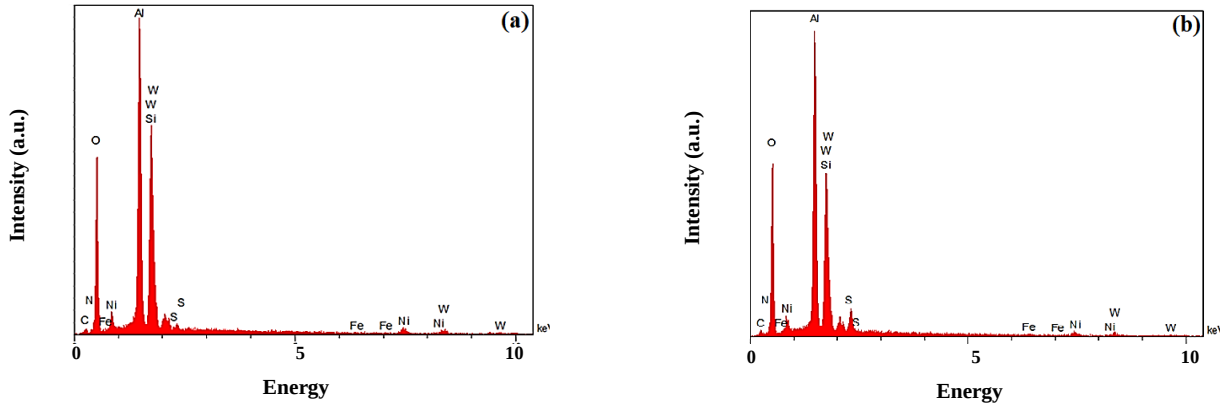

Fig. 7: EDS spectra of (a) fresh and (b) regenerated catalysts.

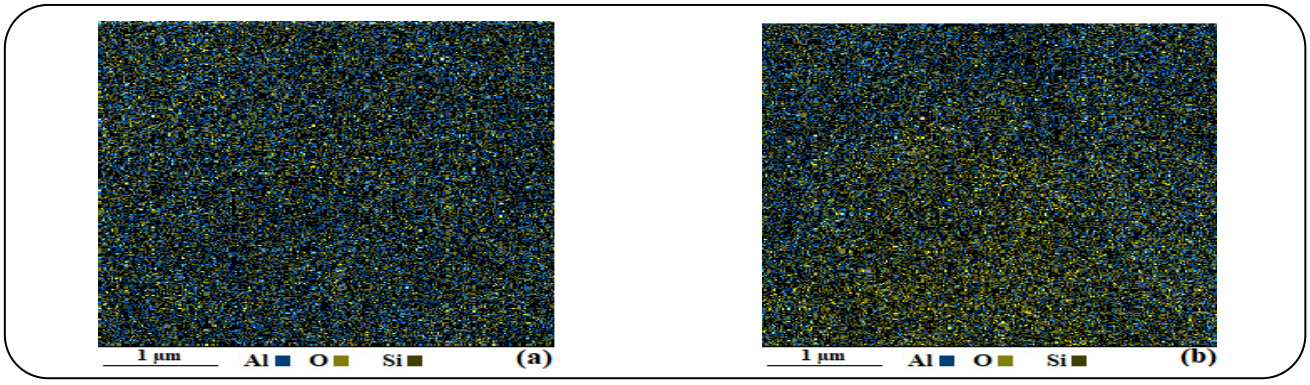

Fig. 1: Elemental mapping of the main elements of support (a) fresh and (b) regenerated.

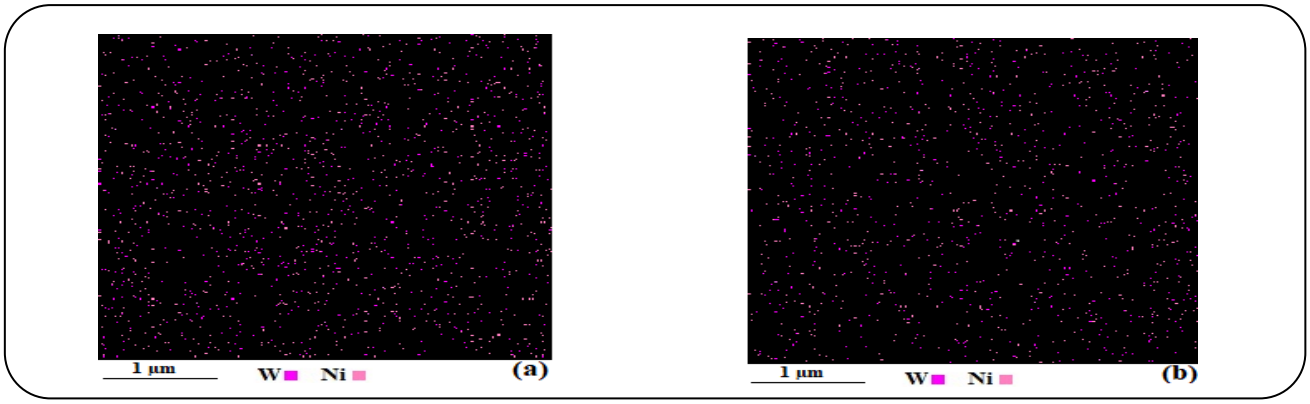

Fig. 2: Elemental mapping of the main elements of active metals phase (a) fresh and (b) regenerated.

main peaks are seen. The first one is in the range of 0-179 °C that belongs to the physical removal of water molecules and adsorbed moisture, indicating weight loss of 3.54%. The second peak is at 274 °C, which is related to the removal of water of crystallization, oxidizing of the catalyst, and the thermal deterioration of the NiO group [50]. The third peak is at 516 °C, showing initiation of thermal degradation and sintering or interaction between Ni and W of the fresh catalyst. As the normal temperature of operation in the hydrocracking process is between (380-440) °C, therefore, any local temperature increase over this range of temperature would lead to sintering and thermal degradation of the catalyst. In the DTA-curve, there is an endothermic peak that confirms the physical removal of water molecules and adsorbed moisture by absorbing heat. Also, the DTA of 274 and 516 °C is shown two exothermic peaks.

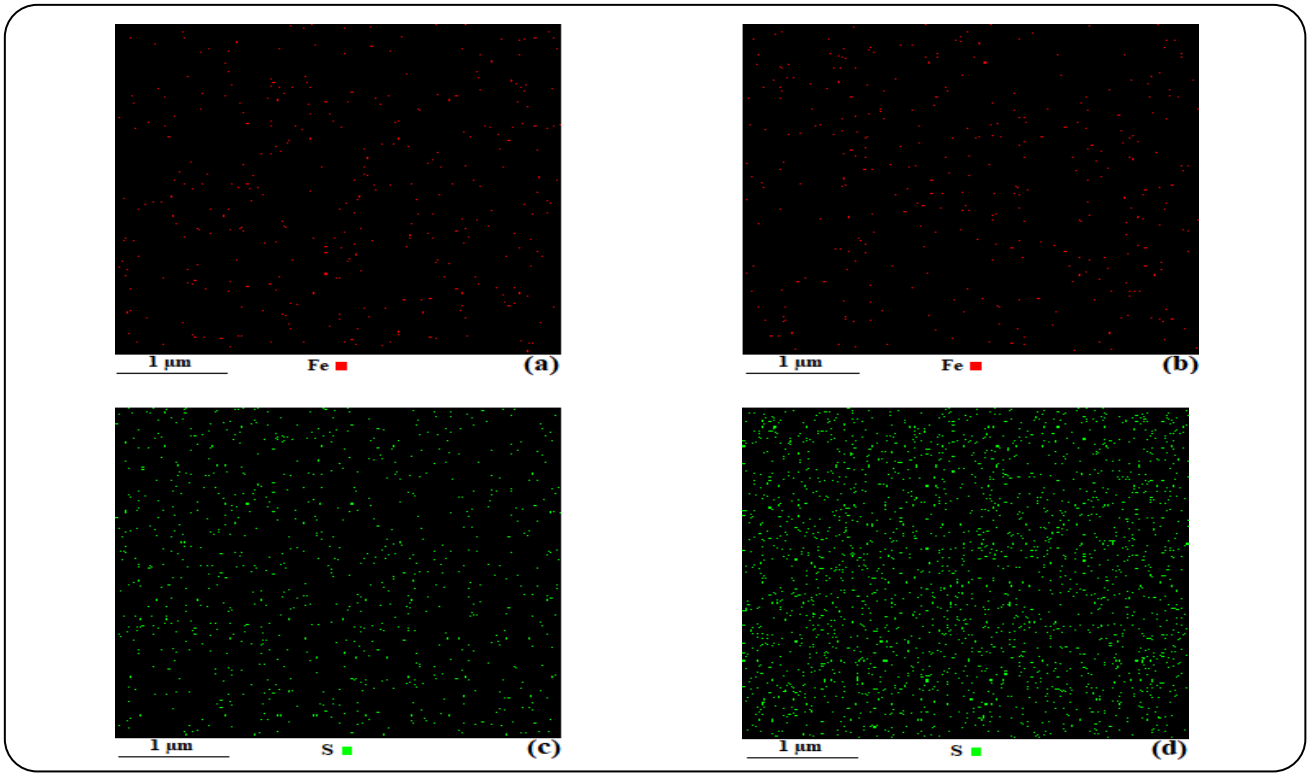

Fig. 3: Elemental mapping of Fe and S for the fresh and regenerated catalysts (a) Fe-fresh, (b) Fe-regenerated, (c) S-fresh and (d) S-regenerated.

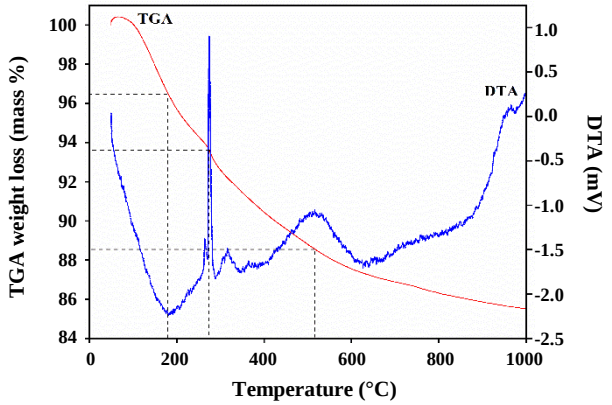

Fig. 11: TGA and DTA of the fresh catalyst in the O_2 atmosphere.

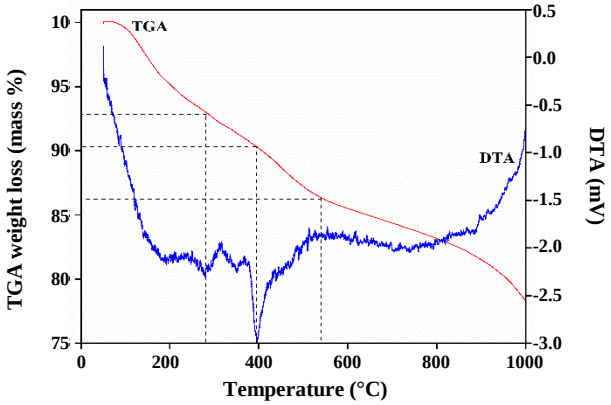

Fig. 12: TGA and DTA of the regenerated catalyst in the Ar atmosphere.

TGA-DTA of the regenerated sample was made in the presence of the Ar atmosphere, which its results are presented in Fig. 12. The first step of weight loss is at 0-280 °C, which is an indication of the physical removal of water molecules, adsorbed moisture, and impurities deposited on the surface of the catalyst [32]. The second peak occurs at 392 °C, which belongs to more destruction of organic fragments [51]. The last peak is at 540 °C, indicating the initiation of sintering and thermal degradation. Also, DTA-curve is shown two endothermic peaks of 280 and 392 °C, which belong to physical removal of water molecules and adsorbed moisture, and removal of water of crystallization and hydroxide phases by absorbing heat.

By comparison between fresh and regenerated catalysts, it is found that weight loss in the regenerated sample was more than the fresh sample. The reason is probably due to the presence of impurities and pollutants deposited on the surface of the catalyst. Therefore, these impurities must also be removed by increasing the temperature during the TGA-DTA process. Increasing the temperature over 440 °C may lead to sintering and thermal degradation, which was considered as not acceptable phenomena for catalyst activity.

CONCLUSIONS

The main objectives of the study were to differentiate comparatively the characteristics of fresh and a three-year used industrial catalysts from the hydrocracking unit of an Iranian refinery and to describe the phenomena affecting the trend towards their deactivation. The results show that the support compositions (Al_2O_3 and Y-zeolite) did not significantly change, but the active metal compositions (NiO and WO_3 or $NiWO_4$) were altered. This alteration was mostly due to the attack of poisoning elements such as outsources V, Pb, Sb, S, and Fe to the active metals. EDS results also exhibited the reduction of Ni and W and increasing of Fe and S in the fresh samples as compared to regenerated one. According to the BJH adsorption/desorption analysis, the total pore volume and specific surface area were reduced from 287.73 m^2/g and 0.46 cm^3/g to 160.84 m^2/g and 0.460 cm^3/g for fresh and regenerated samples, respectively, representing filling the pores with unwanted materials and/or sintering of the primary particle contacts. FESEM images indicated the corroded and indented surface failure of the regenerated catalyst. All analyses confirm the increasing trend of the poisoning and the structural breakdown of the catalysts towards complete deactivation. However, due to the results, the presence of pollutants causes the deactivation of the catalyst, which can be prevented by purifying the feed prior to entering the reactor.

Acknowledgments

The authors thankfully acknowledge the engineering team of the Esfahan Oil Refining Company (EORC) for their support and help in this study by preparing the catalysts samples and operational information from the hydrocracking unit. This work was supported by Abadan Oil Refining Company (AORC) [grant numbers 282].

Received : Sep. 5, 2020 ; Accepted : Dec. 7, 2020

REFERENCES

[1] Choudhary N., Saraf D., Hydrocracking: A Review, *Ind. Eng. Chem. Prod. Res. Dev*, **14(2)**: 74–83 (1975).

[2] Mohanty S., Kunzru D., Saraf D., Hydrocracking: A Review, *Fuel*, 69(12): 1467–1473 (1990).

[3] Sahu R., Song B.J., Im J.S., Jeon Y.P., Lee C.W., A Review Of Recent Advances In Catalytic Hydrocracking Of Heavy Residues, *Ind. Eng. Chem*, **27**: 12–24 (1975).

[4] Hočevar B., Grilc M., Huš M., Likozar B., Mechanism, ab Initio Calculations and Microkinetics of Straight-Chain Alcohol, Ether, Ester, Aldehyde and Carboxylic Acid Hydrodeoxygenation over Ni-Mo Catalyst, *Chem. Eng. J*, **35**: 1339-1351 (2019).

[5] Grilc M., Likozar B., Levec J., Hydrotreatment of Solvolytically Liquefied Lignocellulosic Biomass over $NiMo/Al_2O_3$ Catalyst: Reaction Mechanism, Hydrodeoxygenation Kinetics and Mass Transfer Model Based on FTIR, *Biomass Bioenergy*, **63**: 300-312 (2014).

[6] Ward J.W., Hydrocracking Processes and Catalysts, *Fuel Process. Technol*, **35(1-2)**: 55–85 (1993).

[7] Hočevar B., Grilc M., Huš M., Likozar B., Mechanism, ab Initio Calculations and Microkinetics of Hydrogenation, Hydrodeoxygenation, Double Bond Migration and Cis–Trans Isomerisation During Hydrotreatment of C6 Secondary Alcohol Species and Ketones, *Appl. Catal., B*, **218**: 147-162 (2017).

[8] Minderhoud J., Van Veen J., First-Stage Hydrocracking: Process and Catalytic Aspects, *Fuel Process. Technol*, **35(1-2)**: 87–110 (1993).

[9] Furimsky E., Selection of Catalysts and Reactors for Hydroprocessing, *Appl. Catal. A Gen*, **171(2)**: 177–206 (1998).

[10] Ferraz S.G., Zotin F.M.Z., Araujo L.R.R., Zotin J.L., Influence of support acidity of NiMoS catalysts in the activity for hydrogenation and hydrocracking of tetralin, *Appl. Catal. A Gen*, 384(1-2): 51–57 (2010).

[11] Pookote S., Dranoff J., Butt J., In Hydrogenation Function of Fresh and Deactivated Hydrocracking Catalysts: Cyclohexene Hydrogenation, *ACS Symp. Ser., Chem. React. Engng l, ACS*, **24**: 283-295 (1982).

[12] Fatemi S., Abolhamd G., Mousavian S.M.A., Mortazavi Y.E., The Effect of Coking on Kinetics of HDS Reaction under Steady and Transient States, *Iran. J. Chem. Chem. Eng. (IJCCE)*, **23(2)**: 1-11 (2004).

[13] Gosselink J., Stork W., Coping with Catalyst Deactivation in Hydrocracking: Catalyst and Process Development, *Ind. Eng. Chem. Res*, **36(8)**: 3354–3359 (1997).

[14] Furimsky E., Massoth F.E., Deactivation of Hydroprocessing Catalysts, *Catal. Today*, **52(4)**: 381–495 (1999).

[15] Dufresne P., Hydroprocessing Catalysts Regeneration and Recycling, *Appl. Catal. A Gen*, **322**: 67–75 (2007).

[16] Barghi B., Fattahi M., Khorasheh F., Kinetic Modeling of Propane Dehydrogenation over an Industrial Catalyst in the Presence of Oxygenated Compounds, *React. Kinet., Mech. Catal*, **107(1)**: 141-155 (2012).

[17] Fattahi M., Khorasheh F., Sahebdelfar S., Zangeneh F.T., Ganji K., Saeedizad M., The Effect of Oxygenate Additives on the Performance of Pt–Sn/γ-Al_2O_3 Catalyst in the Propane Dehydrogenation Process, *Sci. Iran*, **18(6)**: 1377-1383 (2011).

[18] Vogelaar B.M., Gast J., Douma E.M., van Langeveld A.D., Eijsbouts S., Moulijn J.A., Coke Deposition Profiles During Artificial Aging of Hydroprocessing Catalysts, *Ind. Eng. Chem. Res*, **46(2)**: 421–429 (2007).

[19] Castaño P., Gutiérrez A., Hita I., Arandes J.M., Aguayo A.s.T., Bilbao J., Deactivating Species Deposited on Pt–Pd Catalysts in the Hydrocracking of Light-Cycle Oil, *Energy and Fuels*, **26(3)**: 1509–1519 (2012).

[20] Sahoo S.K., Ray S.S., Singh I., Structural Characterization of Coke on Spent Hydroprocessing Catalysts Used for Processing of Vacuum Gas Oils, *Appl. Catal. A Gen*, **278(1)**: 83–91 (2004).

[21] Scherzer J., Gruia, A.J., "Hydrocracking Science and Technology", Crc Press, Des Plaines, Illinois (1996).

[22] Samavati A., Fattahi M., Khorasheh F., Modeling of Pt-Sn/γ-Al_2O_3 Deactivation in Propane Dehydrogenation with Oxygenated Additives, *Korean J. Chem. Eng.*, **30(1)**: 55-61 (2013).

[23] Ferella F., A Review on Management and Recycling of Spent Selective Catalytic Reduction Catalysts, *J. Cleaner Prod*, 118990, (2019).

[24] Barghi B., Fattahi M., Khorasheh F., The Modeling of Kinetics and Catalyst Deactivation in Propane Dehydrogenation over Pt-Sn/γ-Al_2O_3 in Presence of Water as an Oxygenated Additive, *Pet. Sci. Technol*, **32(10)**: 1139-1149 (2014).

[25] Marafi M., Furimsky E., Hydroprocessing Catalysts Containing Noble Metals: Deactivation, Regeneration, Metals Reclamation, and Environment and Safety, *Energy and Fuels*, **31(6)**: 5711–5750 (2017).

[26] Dufresne P., Brahma N., Off- site Regeneration of Hydroprocessing Catalysts, *Bull. Des Sociétés Chim. Belges*, 104(4-5): 339–346 (1995).

[27] Teixeira da Silva V., Lima F., Dieguez L., Schmal M., Regeneration of a Deactivated Hydrotreating Catalyst, *Ind. Eng. Chem. Res*, **37(3)**: 882–886 (1998).

[28] Brunauer S., Emmett P.H., Teller E., Adsorption of Gases in Multimolecular Layers, *J. Am. Chem. Soc*, **60(2)**: 309–319 (1938).

[29] Barrett E.P., Joyner L.G., Halenda P.P., The Determination of Pore Volume and Area Distributions in Porous Substances. I. Computations from Nitrogen Isotherms, *Am. Chem. Soc*, **73(1)**: 373–380 (1951).

[30] Lazić M., Hadnađev M., Bošković G., Obadović D., Kiss E., Influence of Excess Sodium Ions on the Specific Surface Area Formation in a NiO-Al_2O_3 Catalyst Prepared by Different Methods, *Sci. Sinter*, **40(2)**: 175–184 (2008).

[31] Boscagli C.,Yang C., Welle A., Wang W., Behrens S., Raffelt K., Grunwaldt J-D., Effect of Pyrolysis Oil Components on the Activity and Selectivity of Nickel-Based Catalysts During Hydrotreatment, *Appl. Catal. A Gen*, **544**: 161-172 (2017).

[32] Kohli K., Prajapati R., Maity S., Sau M., Garg M., Deactivation of Hydrotreating Catalyst By Metals in Resin and Asphaltene Parts of Heavy Oil and Residues, *Fuel*, **175**: 264-273 (2016).

[33] Subsadsana M., Kham-or P., Sangdara P., Suwannasom P., Ruangviriyachai C., Synthesis and Catalytic Performance of Bimetallic NiMo-and NiW-ZSM-5/MCM-41 Composites for Production of Liquid biofuels, *J. Fuel Chem. Technol*, **45(7)**: 805-816 (2017).

[34] Adhikari S., Fernando S.D., To S.F., Bricka R.M., Steele P.H., Haryanto A., Conversion of Glycerol to Hydrogen *via* a Steam Reforming Process over Nickel Catalysts, *Energy and Fuels*, **22(2)**: 1220–1226 (2008).

[35] Xiao Z-q., Mao J.-W., Ji J.-b., Sha R.-y., Yu F., Chuang X., Preparation of Nano-Scale Nickel-Tungsten Catalysts by pH Value Control and Application in Hydrogenolysis of Cellulose to Polyols, *J. Fuel Chem. Technol*, **45(6)**: 641-650 (2017).

[36] Xiao Z-q., Zhang Q., Wang X.-L., Ge Q., Gai X.-k., Mao J.-w., Ji J.-b., Organic Nitrogen Promotes Stability of Metallic Catalysts In Conversion of Bamboo Pulp to Low Carbon Polyols, *J. Fuel Chem. Technol*, **47(6)**: 675-687 (2019).

[37] Sing K.S., Reporting Physisorption Data for Gas/Solid Systems with Special Reference to the Determination of Surface Area and Porosity (Recommendations 1984), *Pure Appl. Chem.*, **57(4)**: 603–619 (1985).

[38] Ramesh A., Tamizhdurai P., Krishnan P.S., Ponnusamy V.K., Sakthinathan S., Shanthi K., Catalytic Transformation of Non-Edible Oils to Biofuels Through Hydrodeoxygenation Using Mo-Ni/Mesoporous Alumina-Silica Catalysts, *Fuel*, **262**: 116494 (2020).

[39] Li Y., Pan D., Yu C., Fan Y., Bao X., Synthesis and Hydrodesulfurization Properties of NiW Catalyst Supported on High-Aluminum-Content, Highly Ordered, and Hydrothermally Stable Al-SBA-15, *J. Catal*, **286**: 124–136 (2012).

[40] Badoga S., Sharma R.V., Dalai A.K., Adjaye J., Synthesis and Characterization of Mesoporous Aluminas with Different Pore Sizes: Application in Nimo Supported Catalyst for Hydrotreating of Heavy Gas Oil, *Appl. Catal. A Gen*, **489**: 86–97 (2015).

[41] Bozdag A.A., Kaynar A.D., Dogu T., Sezgi N., Development of Ceria and Tungsten Promoted Nickel/Alumina Catalysts for Steam Reforming of Diesel, *Chem. Eng. J*, **377**: 120274 (2019).

[42] Jahromi H., Agblevor F.A., Hydrotreating of Guaiacol: A Comparative Study of Red Mud-Supported Nickel and Commercial Ni/SiO_2-Al_2O_3 Catalysts, *Appl. Catal. A Gen*, **558**: 109-121 (2018).

[43] Wang L., Zhu S., Marinkovic N., Kattel S., Shao M., Yang B., Chen J.G., Insight into the Synergistic Effect Between Nickel and Tungsten Carbide for Catalyzing Urea Electrooxidation in Alkaline Electrolyte, *Appl. Catal., B*, **232**: 365-370 (2018).

[44] El-Kemary M., Nagy N., El-Mehasseb I., Nickel Oxide Nanoparticles: Synthesis and Spectral Studies Of Interactions with Glucose, *Mater. Sci. Semicond. Process*, **16(6)**: 1747-1752 (2013).

[45] Díaz-Reyes J., Dorantes-García V., Pérez-Benítez A., Balderas-López J.A., Obtaining of Films of Tungsten Trioxide (WO_3) by Resistive Heating of a Tungsten Filament, *Superficies Vacio*, **21(2)**: 12-17 (2008).

[46] Cardoso F.P., Nogueira A.E, Patrício P.S.O, and Oliveira L.C.A., Effect of Tungsten Doping on Catalytic Properties of Niobium Oxide, *J. Braz. Chem. Soc*, 23(4): 702-709 (2012).

[47] Atanasova P., Tabakova T., Vladov C., Halachev T., Agudo A.L., Effect of Phosphorus Concentration and Method of Preparation on the Structure of the Oxide Form of Phosphorus-Nickel-Tungsten/Alumina Hydrotreating Catalysts, *Appl. Catal. A Gen*, **161(1-2)**: 105-119 (1997).

[48] Rahdar A., Aliahmad M., Azizi Y., NiO Nanoparticles: Synthesis and Characterization, *J. Nanostruct*, **5(2)**: 145-151 (2015).

[49] Davar F., Fereshteh Z., Salavati-Niasari M., Nanoparticles Ni and NiO: Synthesis, Characterization and Magnetic Properties, *J. Alloys Compd*, **476(1-2)**: 797-801 (2009).

[50] Hernández I.P., Gochi-Ponce Y., Larios J.L.C., Fernández A.M., Steam Reforming of Ethanol over Nickel-Tungsten Catalyst, *Int. J. Hydrogen Energy*, **35(21)**: 12098-12104 (2010).

[51] Pereyma V.Y., Klimov O.V., Prosvirin I.P., Gerasimov E.Y., Yashnik S.A., Noskov A.S, Effect of Thermal Treatment on Morphology and Catalytic Performance of NiW/Al_2O_3 Catalysts Prepared Using Citric Acid as Chelating Agent, *Catal. Today*, **305**: 162-170 (2018).